J Mater Sci (2012) 47:132–137
DOI 10.1007/s10853-011-5779-y

Magnetic and luminescent properties of Fe_3O_4@Y_2O_3:Eu^{3+} nanocomposites

Lizhu Tong · Deming Liu · Jianhui Shi · Xuwei Yang · Hua Yang

Received: 27 May 2011 / Accepted: 8 July 2011 / Published online: 20 July 2011
© Springer Science+Business Media, LLC 2011

Abstract The multifunctional Fe_3O_4@Y_2O_3:Eu^{3+} nanocomposites were prepared by a facile solvothermal method with Fe_3O_4 nanoparticles as the core and europium-doped yttrium oxide (Y_2O_3:Eu^{3+}) as the shell. It is shown that Fe_3O_4@Y_2O_3:Eu^{3+} nanocomposites have a strong photoluminescence and special saturation magnetization Ms of 6.1 emu/g at room temperature. The effects of the magnetic field on the luminescence intensities of the nanocomposites are being discussed. The multifunctional nanocomposites with magnetic resonance response and fluorescence probe properties may be useful in biomedical applications, such as cell separation and bioimaging.

Introduction

For the last two decades, the interest in developing materials has culminated especially in the preparation of high quality materials with enhanced functionality. Multifunctional nanocomposites that possess desirable properties in a single entity have attracted broad interest in recent years. For instance, the nanocomposites with both fluorescent and magnetic properties can be used in a wide range of applications in biological systems, such as bioimaging, diagnostic, and therapeutics. They can serve as luminescent markers; and they can also be controlled by an external magnetic field. Most of the magnetic fluorescent nanocomposites are core–shell structures with the great majority of emitters being either quantum dots (QDs) or organic dyes [1–5].

L. Tong · D. Liu · J. Shi · X. Yang · H. Yang (✉)
College of Chemistry, Jilin University, Changchun 130012, China
e-mail: huayang86@sina.com

To the best of our knowledge, the combination of magnetic and fluorescent properties into a single micro or nanocomposite material may greatly enhance the applications of the material in the biomedical and biopharmaceutical fields [6, 7]. A number of methods have been developed for the synthesis of composite microspheres with magnetic and fluorescent properties. Most of the magnetic and fluorescent nanocomposites are core–shell structures with the magnetic particles as the core and the fluorescent phosphors as the shell [8–17].A class of highly fluorescent and magnetic core–shell nanocomposite in the submicrometer size range was synthesized by a modified solvothermal method. Till date, there are few examples of truly multifunctional behaviors (coexistence of magnetic and fluorescent properties) through core–shell engineering [16, 18–27]. Lu et al. [28] deposited a shell of up-converting phosphor on an iron oxide core. Ian M. Kennedy et al. synthesized multifunctional Fe_3O_4@Y_2O_3:Eu^{3+} nanocomposites by a facile homogenous precipitation method. However, the relationship between the magnetic and fluorescent properties, the energy changes of the magnetic and fluorescent properties under the UV light irradiation, and the magnetic field effects are discussed little. Furthermore, most of the crystal systems for Iron oxidation magnetic materials (which are stable during reaction) exist in a cubic system, while oxide-based semiconductor materials exist in a hexagonal system. The large variation in lattice parameter for these two crystal systems strictly promotes the formation of an alloy rather than an overgrowth process. Consequently, all these obstacles have limited the syntheses and studies of these truly multifunctional NCs. Hence, it is crucial to find a synthetic approach that is highly effective in preparing core–shell multifunctional NCs.

In this article, we report the development of a facile solvothermal method for the synthesis of multifunctional nanocomposites with Fe_3O_4 nanoparticles as the core and the Y_2O_3:Eu^{3+}as the shell. Then, we discussed the relationship between the magnetic and fluorescent properties.

Experimental section

Materials

All the chemicals were of analytical grade and were used as received without further purification. Deionized water was used. Ferrous chloride $FeCl_3 \cdot 6H_2O$, HCl (analytical reagent, A. R., Beijing Fine Chemical Company, China), CH_3COONa (A. R. Beijing Fine Chemical Company, China), Ln_2O_3 (Y_2O_3, Eu_2O_3 purity >99.99%) were all purchased from the Beijing Chemical Reagent Company, and ethylene glycol (EG) and ethanol from A.R., Beijing Fine Chemical Company, China.

Synthesis of Fe_3O_4 nanoparticles

$FeCl_3 \cdot 6H_2O$ (1.35 g, 5 mmol) was dissolved in ethylene glycol (40 mL) to form a clear solution, followed by the addition of NaAc (3.6 g) and polyethylene glycol-20000 (1.0 g). The mixture was stirred vigorously for 30 min, and then sealed in a teflon-lined stainless steel autoclave (50-mL capacity). The autoclave was heated to and maintained at 200 °C for 8–12 h, and allowed to cool at room temperature. The black products were washed several times with ethanol and dried at 80 °C for 12 h.

Synthesis of Fe_3O_4@Y_2O_3:Eu^{3+} nanocomposites

In a typical synthesis, 0.97 mmol Y_2O_3 and 0.03 mmol Eu_2O_3 were dissolved in dilute HCl, resulting in the formation of a colorless solution of YCl_3 and $EuCl_3$. After evaporation followed by drying at 80 °C for 5 h in ambient atmosphere, a powder mixture of YCl_3 and $EuCl_3$ was obtained. Then 2.0 g CH_3COONa and 37 mL mixing solution of ethylene glycol (EG) and water (volume ratio for EG:H_2O is 35:2) were added to the mixture of YCl_3 and $EuCl_3$. Add 0.077 g of Fe_3O_4 into the mixture solution, and then stirred for another 3 h. Then the transparent feedstock was charged into a 45 mL Teflon-lined stainless autoclave and heated at 180 °C for 8 h. After the autoclave was cooled to room temperature naturally, the precursors were separated by filtration, washing with ethanol and distilled water several times, and drying in atmosphere at 50 °C for 12 h. The final products were retrieved through a heat treatment at desired temperatures (700–800 °C) in air for 3 h.

Characterization

The purities of all the samples were checked by X-ray diffraction measurements at room temperature using CuKα radiation (Kα = 1.54059 Å). A spectrophotometer (Hitachi F-4500 spectrouorimeter equipped with a 150 W xenon lamp as the excitation source) was used for the photoluminescent (PL) measurement at room temperature. The morphology and microscope were characterized using scanning electronic microscope (SEM, Philps XL-30). The room temperature magnetic hysteresis (M–H) loops were measured employing a vibrating sample magnetometry (VSM) system (JDM-13) using a maximum magnetic field of 10000 Oe.

Results and discussion

Figure 1 shows SEM images of Fe_3O_4 and Fe_3O_4@Y_2O_3:Eu^{3+} nanoparticles. It can be seen that the Fe_3O_4 particles are almost spherical with the average diameters of about 200 nm in Fig. 1a. Although the particles should remain discrete entities due to the high steric exclusion properties of PEG hydrophilic chains located at the surface of the nanoparticles, there was still some apparent aggregation in the SEM images, which might be because of the

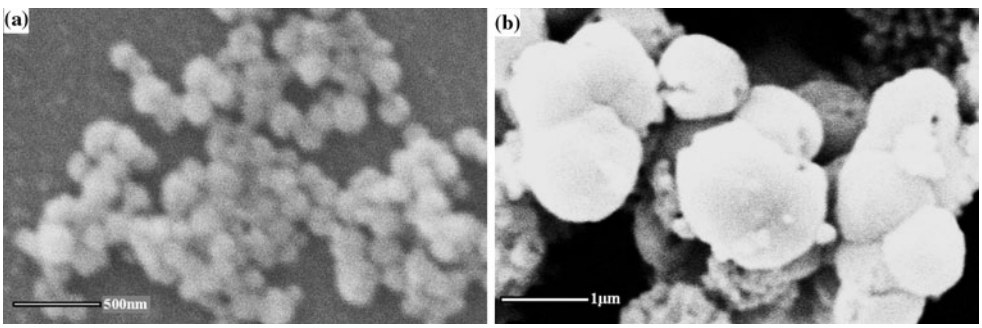

Fig. 1 SEM images of Fe_3O_4 (**a**) and Fe_3O_4@Y_2O_3:Eu^{3+} (**b**)

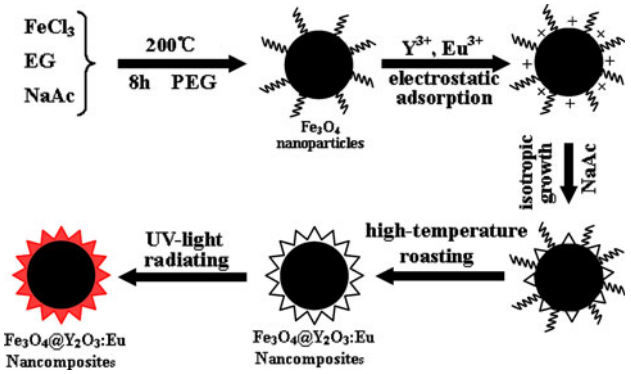

Scheme 1 Illustration for the formation process of the spherical $Fe_3O_4@Y_2O_3:Eu^{3+}$ nanocomposites

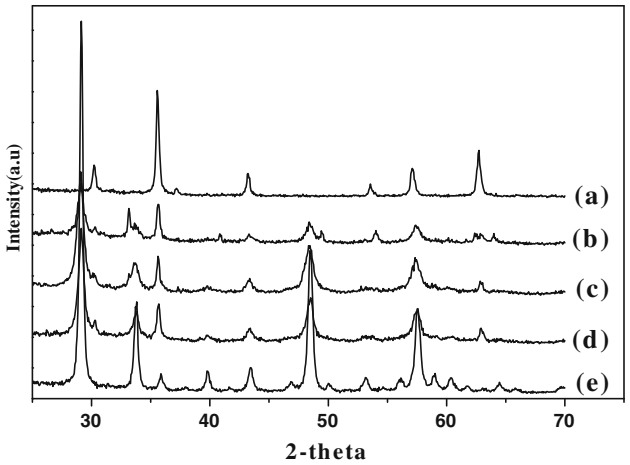

Fig. 2 XRD patterns of Fe_3O_4 (*a*), $Fe_3O_4@$ $Y_2O_3:Eu^{3+}$ (*b–d*), and $Y_2O_3:Eu^{3+}$ (*e*) (*R* of *b–e*: 1:5, 1:3, 1:1; 0, R = the mass ratios of $Fe_3O_4/Y_2O_3:Eu^{3+}$)

cross-linkage of the PEG chains due to hydrogen bonding; SEM sample preparation and drying can also lead to apparent aggregation. Figure 1b shows a SEM image of $Fe_3O_4@Y_2O_3:Eu^{3+}$. The SEM images indicate that these nanocomposites are spherical in shape and uniform in size. The diameter of the nanocomposites is mainly centered at 1 μm. The SEM image also reveals the surface configuration of the microspheres [29]. The spherical microsphere implies that these microspheres may be comprised of smaller subunits. We describe synthesis routes of lumino-magnetic bifunctional microspheres with core–shell structure in Scheme 1.

Figure 2 shows the X-ray diffraction patterns of Fe_3O_4, $Y_2O_3:Eu^{3+}$, and $Fe_3O_4@Y_2O_3:Eu^{3+}$ nanocomposites with the different mass ratios of $Fe_3O_4/Y_2O_3:Eu^{3+}$. It is shown that there are five reflection peaks of the nanocomposites at $2\theta = 20.59°$, 29.12°, 33.78°, 48.50°, and 57.63° correspond to (211), (222), (400), (440), and (622), respectively. They are in good accordance with the JCPDS card No 88-1040 of Y_2O_3 crystals and additional peaks coincide with the XRD peaks of either cubic Fe_3O_4 or γ-Fe_2O_3. Our experimental data cannot clearly distinguish between these two types of iron oxide because they have very similar cubic structure. With the increasing mass ratio of $Fe_3O_4/Y_2O_3:Eu^{3+}$ from 1:1 to 1:5, the XRD peaks intensities of $Y_2O_3:Eu^{3+}$ are sharper and stronger, and ones of cubic Fe_3O_4 are weaker. In addition, no additional peaks for other phases can be detected. The sharp and strong XRD peaks are well confirmed with the crystallization when the mass ratio of $Fe_3O_4/Y_2O_3:Eu^{3+}$ is 1:3. Thus, we chose the mass ratio of $Fe_3O_4/Y_2O_3:Eu^{3+}$ is 1:3.

Figure 3 shows the excitation (left) and emission (right) spectra of $Fe_3O_4@Y_2O_3:Eu^{3+}$ with different concentrations of Eu^{3+} doping which are 3, 7, 10 and 5%. The excitation spectra of $Fe_3O_4@Y_2O_3:Eu^{3+}$ nanocomposites are composed of a broad peak and a series of sharp peaks. The former is due to part of the charge transfer band (CTB) of Eu^{3+}–O^{2-} bond, and latter is from the *f–f* transitions within Eu^{3+} $4f^6$ electron configuration of Eu^{3+} ions. The emission spectra of the nanocomposites were tested at 254 nm. There are a series of sharp lines of the emission spectra of $Y_2O_3:Eu^{3+}$ nanocrystal in the regions of 550–700 nm in Fig. 3 (right). The band at 610 nm is due to the forced electric dipole transition ($^5D_0$–$^7F_2$) of Eu^{3+} ions, which is allowed on condition that the 3*p* electrons of Eu^{3+} ion are occupied as a site without an inverse center. The broad peak at 590 nm derives from the allowed magnetic dipole transition ($^5D_0$–$^7F_1$) of Eu^{3+} ions. Figure 3 shows the effect of the doped Eu^{3+} content in composites on the relative PL intensity. The highest intensity of the emission spectra is at 3 mol% of doped Eu^{3+} concentration. Higher Eu^{3+} contents in nanoparticles led to quenching the PL intensity. Thus, the optimum concentration for doped Eu^{3+} ions in Y_2O_3 host is 3%.

Figure 4 shows the excitation (left) and emission (right) spectra of $Fe_3O_4@Y_2O_3:Eu^{3+}$ nanocomposites with the different mass ratios R of Fe_3O_4 and $Y_2O_3:Eu^{3+}$. Under excitation at 254 nm, there is a red luminescence of $Fe_3O_4@Y_2O_3:Eu^{3+}$ nanocomposites at 610 nm in Fig. 4 (right), which can be assigned to the $^5D_0$–$^7F_2$ transition of Eu^{3+} ions. There is a broad band of the excitation spectrum at 254 nm in Fig. 4 (left), and there are some sharp bands in region of 300–500 nm. The former is due to the charge-transfer band (CTB) of Eu^{3+}–O^{2-}, and the latter is resulted from the *f–f* transition lines of Eu^{3+} ions with weak intensity compared with the Eu^{3+}–O^{2-} CTB [30]. Upon excitation at 254 nm, there are a series emission bands of Eu^{3+} ions in the region of 550–700 nm in Fig. 4 (right). As can be seen from Fig. 3 (right), the emission bands are resulted from $^5D_0 \rightarrow {}^7F_J$ ($J = 0, 1, 2, 3, 4$) transitions of Eu^{3+} ions, and the band of $^5D_0 \rightarrow {}^7F_2$ transition at 610 nm is the most prominent. All the other emission bands at

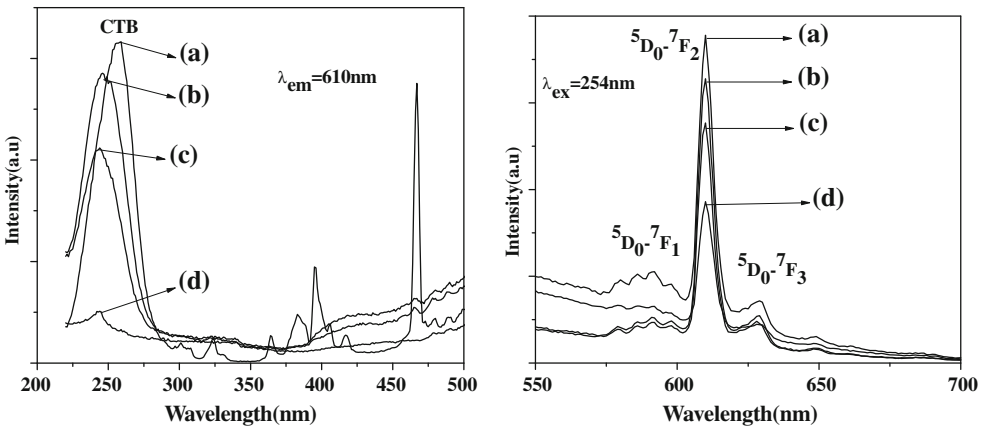

Fig. 3 Excitation (*left*) and emission spectra (*right*) of Fe_3O_4@Y_2O_3:Eu^{3+} with different Eu^{3+} concentrations : *a* 3%; *b* 7%; *c* 10%; *d* 5%

533 nm ($^5D_1 \rightarrow {}^7F_1$), 580 nm ($^5D_0 \rightarrow {}^7F_0$), 586, 592, 599 nm ($^5D_0 \rightarrow {}^7F_1$), 629 nm ($^5D_0 \rightarrow {}^7F_3$), and 706 nm ($^5D_0 \rightarrow {}^7F_4$) are shown in Fig. 4 (right). From Fig. 4, the intensities of both excitation and emission bands of Eu^{3+} ions in Fe_3O_4@Y_2O_3:Eu^{3+} are decreased compared with that of Y_2O_3:Eu^{3+}. Furthermore, with increasing the mass ratio *R* of Fe_3O_4@Y_2O_3:Eu^{3+} from 1:1 to 1:5, the intensities of the excitation and emission bands of Fe_3O_4@Y_2O_3:Eu^{3+} are increased. Fe_3O_4 particles also product some effects to a certain extent. Thus, the intensities of both excitation and emission spectra of Fe_3O_4@Y_2O_3:Eu^{3+} are decreased. Compared with pure Y_2O_3:Eu^{3+} sample, the luminescent intensities of the Fe_3O_4@Y_2O_3:Eu^{3+} nanocomposites are decreased significantly. The magnetic Fe_3O_4, which exhibit a strong quenching effect on the luminescence intensity, caused the decreasing of absorption UV energy of activator ions in host. Therefore, the decreased volume for the photon–solid interaction at the surface of Fe_3O_4@Y_2O_3:Eu^{3+} nanocomposites is a main reason for the decreased emission intensity.

Figure 5 shows the excitation and emission spectra of Fe_3O_4@Y_2O_3:Eu^{3+} nanocomposites under magnetic field. We discussed the effects of the different magnetic fields on the luminescent properties of the nanocomposites under 0.25 T magnetic fields for 0, 1, 3, 4 and 5 h, respectively. As can be seen from the excitation and emission spectra, the luminescent intensities of the nanocomposites are gradually increased from 0 to 3 h, and then gradually decreased. It is supposed that the observed effects are attributed to a strong magnetic field quenching effect on the luminescence intensity of Fe_3O_4@Y_2O_3:Eu^{3+} nanocomposites. In nanocomposite, the inducement begets by the arrangement order of magnetic domains is reduced after magnetic field for 3 h, which lead to reduce in the luminescence intensity. In addition, the electrons of Eu^{3+} in the *d–f* transition process have a directional rearrangement process under the effect of magnetic field. The other reason may be the form of the lattice defects which result in the changing of magnetism, and then further affect the luminescent intensity [31]. Compared with the others under the magnetic field, all the peaks of 0 h did not shift, but the intensity changed. The results showed that the energy of the magnetic Fe_3O_4 was employed to excite more valence electrons of the phosphors to the excited state. The more the valence electron was excited, the stronger the PL intensity was. When the duration reached 3 h, the number of excited valence electrons reached the maximum. The quenching effects will gradually affect more because the

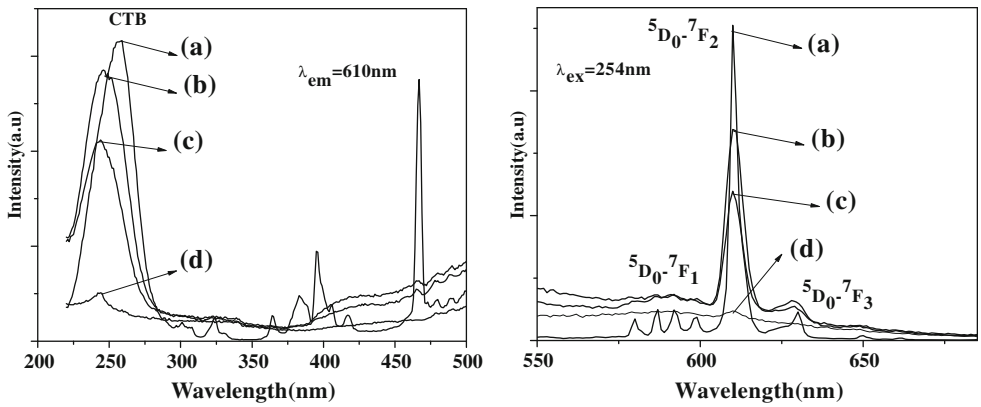

Fig. 4 Excitation (*left*) and emission (*right*) spectra of Y_2O_3:Eu^{3+} (*a*), Fe_3O_4@Y_2O_3:Eu^{3+} (*b–d*) (*R* of *a–d*: 0, 1:5, 1:3, 1:1; *R* = the mass ratios of Fe_3O_4 and Y_2O_3:Eu^{3+})

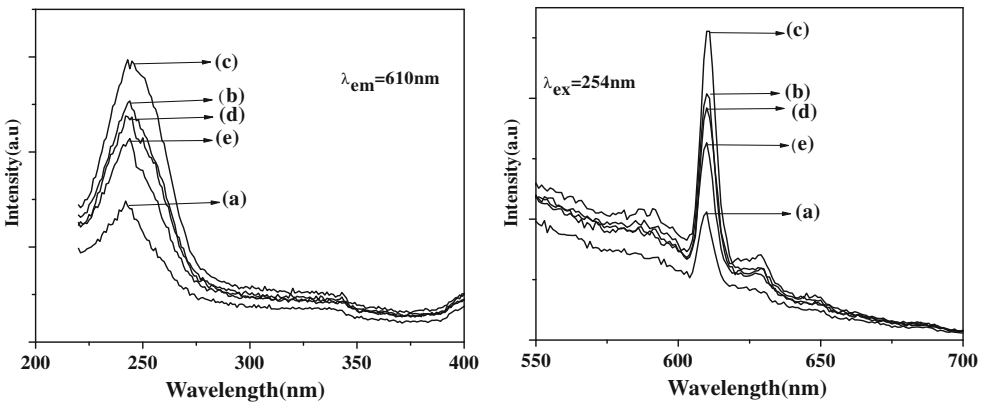

Fig. 5 Excitation (*left*) and emission (*right*) spectra of $Fe_3O_4@Y_2O_3:Eu^{3+}$ under magnetic field for 0 h (*a*); 1 h (*b*); 3 h (*c*); 4 h (*d*); 5 h (*e*)

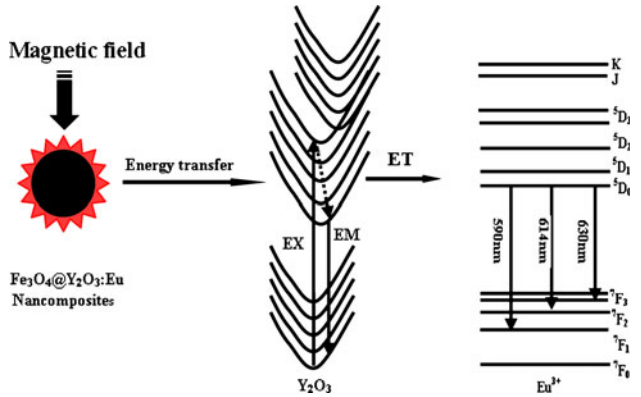

Scheme 2 The mechanism of the modification for the luminescence intensity

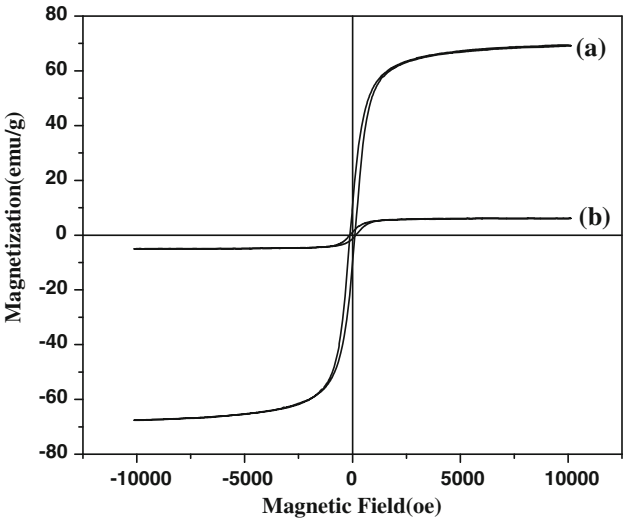

Fig. 6 The magnetic hysteresis loops of Fe_3O_4 (*a*), $Fe_3O_4@Y_2O_3:Eu^{3+}$ (*b*)

magnetite located at an active state. Then the luminescent intensity will gradually decrease. The whole mechanism process was shown in Scheme 2.

The magnetic properties of Fe_3O_4 and $Fe_3O_4@Y_2O_3:Eu^{3+}$ nanocomposites were characterized using a vibrating sample magnetometer (VSM). The magnetization curves of the obtained nanocomposites registered at 300 K shows nearly no residual magnetism is detected in Fig. 6, which means that the nanocomposite exhibited the paramagnetic characteristics. The saturation magnetization values Ms of Fe_3O_4 and $Fe_3O_4@Y_2O_3:Eu^{3+}$ nanocomposites are 69.27 and 6.1 emu/g, respectively. It is clearly seen from these magnetic hysteresis loops that all the samples have stronger magnetism with negligible coercivity and remanence at room temperature. These nanocomposites with paramagnetic characteristics and high saturation magnetization values can quickly respond to the external magnetic field and quickly redisperse once the external magnetic field is removed. The saturation magnetization values Ms of the Fe_3O_4 composite is 69.27 emu/g, which is obviously higher than the bulk Ms 6.1 emu/g of $Fe_3O_4@Y_2O_3:Eu^{3+}$. It can be attributed to a trace amount of metallic, which has the highest magnetic moment among the ferromagnetic Fe_3O_4 transition metals, and which may be the lattice defects result in the orderly arrangement of the magnetic domain in magnetic materials. Otherwise, compared with the uncoated Fe_3O_4 particles, the saturation magnetization of the $Fe_3O_4@Y_2O_3:Eu^{3+}$ microspheres obviously decreased because the diamagnetic contribution of the thick $Y_2O_3:Eu^{3+}$ shell resulted in a low mass fraction of the Fe_3O_4 magnetic substance. Though the saturation magnetization of $Fe_3O_4@Y_2O_3:Eu^{3+}$particles is less than the magnetite nanoparticles as magnetic core, it is strong enough for effective magnetic separation.

Figure 7 shows the photographs of the nanocomposites dispersed in water without and with the magnet field under visible light and UV light at 365 nm. The photograph of the composites without the magnet field under the visible light is shown in Fig. 7a. Figure 7b shows the photograph of the composites with magnet field under UV light. To illustrate dispersibility in aqueous medium and magnetic response to the external magnetic field, a simple experiment was performed which illustrate the mentioned manipulation ability. An optical photograph of the

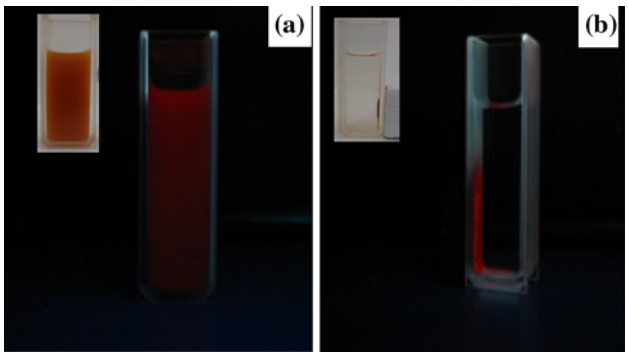

Fig. 7 Photographs of $Fe_3O_4@Y_2O_3:Eu^{3+}$ nanocomposite without (**a**) and with (**b**) magnet field under visible light (**a**) and UV light at 365 nm (**b**)

magnetic microspheres attracted by an external magnet is exhibited in Fig. 7. When a magnet was placed close to the quartz-vial holding the magnetic microspheres dispersed in deionized water, the microspheres were attracted toward the magnet very quickly and accumulated to the side of the quartz-vial near the magnet in 2 min, and the solution became clear and transparent. These nanocomposites with paramagnetic characteristics and high magnetization values can quickly respond to the external magnetic field and quickly redisperse once the external magnetic field is removed. $Fe_3O_4@Y_2O_3:Eu^{3+}$ nanocomposites show the same property under UV light irradiation. This simple experiment confirmed that the magnetic microspheres possess good water-disperse and magnetic separation characteristics.

Conclusions

In summary, multifunctional $Fe_3O_4@Y_2O_3:Eu^{3+}$ nanocomposites with the magnetic and luminescent properties were prepared in a core/shell frame. The optimum mass ratio of $Fe_3O_4/Y_2O_3:Eu^{3+}$ is 1:3, and the optimal concentration for doped Eu^{3+} ions in Y_2O_3 host is 3% which have been examined and verified by various characterization techniques. When the nanocomposites were put under the magnetic field for different times, the luminescent intensities are gradually increased until 3 h, and then gradually decreased with the advantage of high magnetic responsive, unique luminescent properties, high water solubility. We envision that these nanocomposites could be used in a number of biomedical concentration and separation, such as targeting, cell separation, and bioimaging. The proposed strategy for the preparation of complex nanostructures can be extended to other multicomponent materials with similar structures.

Acknowledgements This study is supported by National Natural Science Foundation of China.

References

1. Corr SA, O'Byrne A, Gun'ko YK, Ghosh S, Brougham DF, Mitchell S, Volkov Y, Prina-Mello A (2006) Chem Commun 4474
2. Corr SA, Rakovich YP, Gun'ko YK (2008) Nanoscale Res Lett 3:87
3. Quarta A, Di Corato R, Manna L, Ragusa A, Pellegrino T (2007) IEEE Trans Nanobiosci 6:298
4. Veiseh O, Sun C, Gunn J, Kohler N, Gabikian P, Lee D, Bhattarai N, Ellenbogen R, Sze R, Hallahan A, Olson J, Zhang MQ (2005) Nano Lett 5:1003
5. Yoon TJ, Kim JS, Kim BG, Yu KN, Cho MH, Lee JK (2005) Angew Chem Int Ed 44:1068
6. Levy L, Sahoo Y, Kim K-S, Bergey EJ, Prasad PN (2002) Chem Mater 14:3715
7. Li Y, Yan B, Deng CH, Yu WJ, Xu XQ, Yang PY et al (2007) Proteomics 7:2330
8. Becker C, Hodenius M, Blendinger G, Sechi A, Hieronymus T, Muller-Schulte D, Schmitz-Rode T, Zenke M (2007) J Magn Magn Mater 311:234
9. Hong X, Li J, Wang MJ, Xu JJ, Guo W, Li JH, Bai YB, Li TJ (2004) Chem Mater 16:4022
10. Huh YM, Jun YW, Song HT, Kim S, Choi JS, Lee JH, Yoon S, Kim KS, Shin JS, Suh JS, Cheon J (2005) J Am Chem Soc 127:12387
11. Du GH, Liu ZL, Lu QH, Xia X, Jia LH, Yao KL, Chu Q, Zhang SM (2006) Nanotechnology 17:2850
12. Bertorelle F, Wilhelm C, Roger J, Gazeau F, Menager C, Cabuil V (2006) Langmuir 22:5385
13. Tu CF, Yang YH, Gao MY (2008) Nanotechnology 19:8
14. Gao JH, Zhang B, Gao Y, Pan Y, Zhang XX, Xu B (2007) J Am Chem Soc 129:11928
15. Gu HW, Zheng RK, Zhang XX, Xu B (2004) J Am Chem Soc 126:5664
16. Yoon TJ, Yu KN, Kim E, Kim JS, Kim BG, Yun SH, Sohn BH, Cho MH, Lee JK, Park SB (2006) Small 2:209
17. Lu Y, Yin YD, Mayers BT, Xia YN (2002) Nano Lett 2:183
18. Yi DK, Selvan ST, Lee SS, Papaefthymiou GC, Kundaliya D, Ying JY (2005) J Am Chem Soc 127:4990
19. Giri S, Trewyn BG, Stellmaker MP, Lin VSY (2005) Angew Chem Int Ed 44:5038
20. Zhao WR, Gu JL, Zhang LX, Chen HR, Shi JL (2005) J Am Chem Soc 127:8916
21. Lin YS, Wu SH, Hung Y, Chou YH, Chang C, Lin ML et al (2006) Chem Mater 18:5170
22. Deng YH, Qi DW, Deng CH, Zhang XM, Zhao DY (2008) J AmChemSoc 130:28
23. Kim J, Lee JE, Lee J, Yu JH, Kim BC, An K et al (2006) J Am Chem Soc 128:688
24. Kim JY, Kim HS, Lee NY, Kim TH, Kim HS, Yu TK et al (2008) Angew Chem Int Ed 47:8438
25. Burnsa A, Owb H, Wiesner U (2006) Chem Soc Rev 35:1028
26. Piao YZ, Burns A, Kim JY, Wiesner U, Hyeon T (2008) Adv Funct Mater 18:1
27. Li L, Tsung CK, Ming T, Sun ZH, Ni WH, Shi QH et al (2008) Adv Funct Mater 18:2956
28. Lu HC, Yi GS, Zhao SY, Chen DP, Guo LH, Cheng J (2004) J Mater Chem 14:1336
29. Sordelet D, Akinc M (1988) J Colloid Interface Sci 122:47
30. Song H, Chen B, Peng H, Zhang J (2002) Appl Phys Lett 81:1776
31. Sun Z, Liu D, Tong L, Shi J, Yang X, Yu L, Tao Y, Yang H (2011) Solid State Sci 13:361